Altitudinal Precipitation Gradients in the Tropics from Tropical Rainfall Measuring Mission (TRMM) Precipitation Radar

ALISON M. ANDERS

Department of Geology, University of Illinois at Urbana–Champaign, Champaign, Illinois

STEPHEN W. NESBITT

Department of Atmospheric Sciences, University of Illinois at Urbana–Champaign, Urbana, Illinois

ABSTRACT

A Tropical Rainfall Measuring Mission (TRMM) climatology shows variability in surface precipitation rate–elevation relationships across the tropics. Vertical profiles of radar reflectivity and profiles of specific humidity and cross-barrier moisture fluxes during precipitation events from the Interim European Centre for Medium-Range Weather Forecasts Re-Analysis reveal four precipitation regimes with distinct precipitation mechanisms: 1) a tropical regime with a broad precipitation maximum at ~1500 m where convection is triggered by orographic lifting; 2) a trade winds regime with a near–sea level precipitation maximum dominated by forced ascent due to prevailing winds and the presence of dry air aloft; 3) a wet monsoon regime with a low-elevation precipitation maximum driven by efficient precipitation generation, large low-level cross-barrier moisture fluxes, and multiple convective modes; and 4) a dry monsoon regime with a high-elevation precipitation maximum reflecting intense convection and stratiform rain with a strong evaporation signature. In general, surface precipitation–elevation relationships across the tropics feature lower-elevation precipitation maxima relative to typical midlatitude regimes.

1. Introduction

Large spatial gradients in precipitation are common in mountains (e.g., Anders et al. 2006, 2007; Prat and Barros 2010; Giambelluca et al. 2013) and relevant to diverse fields including hydrology, climatology, hazards assessment, and geomorphology. In the midlatitudes, precipitation rates typically increase with elevation on windward-facing slopes, consistent with stable upslope flow driving progressive rainout (Sawyer 1956; Smith 1979; Roe 2005). In the tropics, precipitation is dominated by convective processes, making the stable upslope model inappropriate. Furthermore, controls on convective precipitation beyond elevation indicate that a single conceptual model may not adequately describe precipitation–elevation relationships across the tropics.

Altitudinal gradients in precipitation across the tropics are variable, including regimes with near–sea level maxima, regimes with moderate-elevation precipitation maxima, and those with approximately uniform precipitation rates (Lauscher 1976; Barry 2008; Colberg and Anders 2014). Lauscher (1976) emphasized associations between precipitation–elevation gradients and latitude, finding a tendency for low-elevation maxima near the equator, moderate-elevation maxima at higher tropical latitudes, and increasing precipitation rates with elevation at midlatitudes. Additionally, high-elevation maxima are associated with drier areas while low-elevation maxima occur in wetter climates (Lauer 1975). These patterns are complicated by local orographic and monsoon circulations and local moisture sources (Barry 2008).

We examine altitudinal precipitation gradients across the tropics in unprecedented detail using Tropical Rainfall Measuring Mission (TRMM) satellite Precipitation Radar (PR) data (1998–2013). These data are compared with profiles of specific humidity and cross-barrier winds during precipitation events from Interim

Corresponding author address: A. Anders, Department of Geology, University of Illinois at Urbana–Champaign, 605 E. Springfield Ave., Champaign, IL 61820.
E-mail: amanders@illinois.edu

TABLE 1. The nine regions studied (see text for full region names). For each region, the geographic coordinates, mountain orientation, and rainy season months are listed.

Region	Lat range	Lon range	Mountain orientation	Wind direction	Rainy season months
MEX	23.623°–31.233°N	112.261°–103.361°W	143.13°	ENE	May–Sep
NAN	12.154°–6.580°S	77.852°–73.136°W	149.04°	ENE	Nov–Mar
NEB	10.500°–4.500°S	38.000°–33.000°W	0°	E	Feb–Jun
AFR	6.000°–16.000°N	35.000°–41.000°E	0°	E	May–Sep
HIM	26.434°–31.902°N	78.250°–86.559°E	109.98°	SSW	May–Sep
WGA	11.449°–18.999°N	72.326°–76.364°E	159.44°	WSW	May–Sep
MYA	15.000°–25.000°N	90.000°–95.500°E	180°	W	May–Sep
NGA	11.000°–1.000°S	132.000°–151.000°E	90°	S	Nov–Mar
EAU	28.000°–33.000°S	149.500°–154.500°E	0°	E	Nov–Mar

European Centre for Medium-Range Weather Forecasts (ECMWF) Re-Analysis (ERA-Interim) data. Our immediate goal is to diagnose the mechanisms behind observed precipitation gradients. Our ultimate goal is to develop a theory of orographic precipitation in the tropics which describes the impacts of humidity, latitude, and monsoon circulations and allows for prediction of precipitation–elevation relationships from event (hours–days) to geomorphic time scales (10^4–10^8 years).

2. Tropical rainfall regimes

Four distinct regimes, which differ in precipitation mechanisms, have been described in the literature. We hypothesize that altitudinal gradients in precipitation will vary among these regimes. The simplest tropical orographic precipitation regime we call the tropical regime. In the absence of other forcing factors, high topography drives a diurnal cycle of convection through heating of the elevated land surface and, possibly, onshore flow. Examples of the tropical regime come from New Guinea, where convective precipitation associated with diurnal heating dominates seasonally (Barry 2008), and the northern and central Andes (Figueroa and Nobre 1990).

A second regime has been described at latitudes between ~10° and 30° from the equator. Here, easterly trade winds impinge on mountain ranges, causing upslope flow and triggering convection. The trade wind inversion influences precipitation processes by limiting the depth of convection. Hawaiian precipitation maxima are located at or below ~2000 m elevation, near the trade wind inversion (Giambelluca et al. 2013). Trade winds are uplifted along the eastern Australian (Sumner and Bonell 1986) and northeastern Brazilian coasts, where flow impinging on topography causes precipitation (Kousky 1980; Rao et al. 1993).

Finally, monsoon circulations generate precipitation in the tropics in India (Gadgil 2003), Southeast Asia (Goswami et al. 1999), Africa (Nicholson 2000), South America (Zhou and Lau 1998), and Mexico and the southwestern United States (Adams and Comrie 1997; Nesbitt et al. 2008). Detailed analysis of the precipitation mechanisms associated with monsoons is beyond the scope of this paper. Factors including the strength of the monsoon circulation and low-level moisture play a role in the spatial distribution of precipitation under this regime. We divide monsoon-influenced areas into two regimes—wet and dry—based on low-level precipitation rates. Wet monsoon regimes experience significant precipitation from near–sea level convective clouds while dry monsoon regimes lack the low-level moisture to produce precipitation at low elevations.

3. Methods

a. Precipitation

We use a 0.05° resolution grid of average near-surface rain rates from TRMM PR 2A25, version 7, for the years 1998–2013; the expanded dataset decreases sampling errors by ~30% relative to the errors reported by Nesbitt and Anders (2009) for the 1998–2007 time period. TRMM PR 2A25 data are superior to blended products, such as TRMM 3B42, for constraining climatological patterns of precipitation in complex terrain because of the errors inherent in infrared, passive microwave, and gauge-correction techniques, which are precipitation process and elevation dependent (e.g., Gochis et al. 2009). Data were considered only during a 5-month-long wet season centered on the peak monthly rainfall accumulation (see Table 1).

Nine regions were selected for examination of the relationship between precipitation and topography (Fig. 1). These include Mexico's Sierra Madre Occidental (MEX), the Peruvian Andes (NAN), the Borborema Plateau in northeastern Brazil (NEB), the Ethiopian Highlands (AFR), the Himalayas (HIM), India's Western Ghats (WGA), Myanmar (MYA), New Guinea (NGA), and the Great Dividing Range of eastern Australia (EAU). In
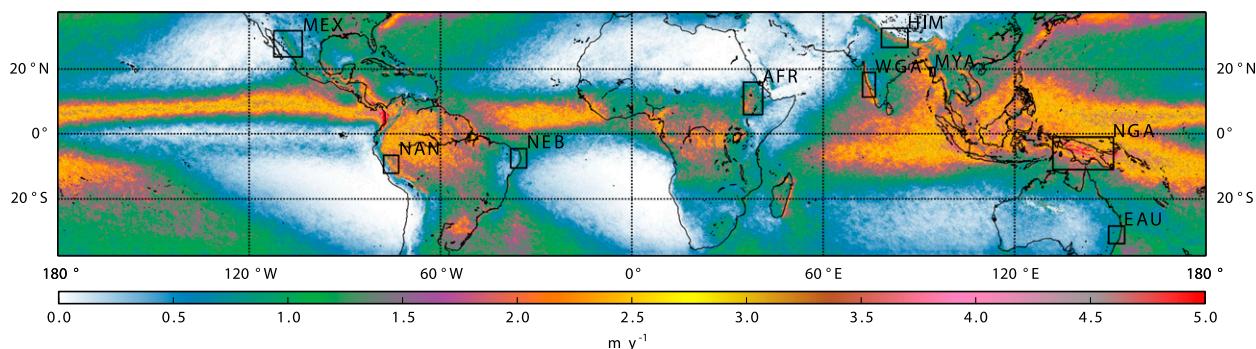
FIG. 1. The 15-yr TRMM PR climatology with the nine labeled study areas (see text for full region names) marked with black boxes.

each region, a study area was defined along and upwind of a segment of topography with a relatively straight crest. In NGA, the study area included areas both north and south of the topographic crest. Pixels were ranked according to their elevations from the TRMM elevation model. The median sea level precipitation was defined by considering all pixels at zero elevation. Elevation bins were defined to include 100 observations. In each bin, the histogram of surface precipitation rates was evaluated and the median surface precipitation rate was associated with the median elevation.

To examine the physical mechanisms generating precipitation in each region, we examined the vertical structure of precipitation using reflectivity profiles from TRMM PR. Attenuation-corrected radar reflectivities from TRMM PR 2A25, version 7, were binned into contour frequency by altitude diagrams (CFADs), corrected for slant angle and the TRMM altitude boost in August 2001, and separated into convective, stratiform, and other based on the classification scheme in PR algorithm 2A23, version 7 (all classification subcategories are combined). In this study, other are added to the convective category; these profiles appeared mostly as shallow convection and nonprecipitating elevated anvils above 10 km.

b. Atmospheric conditions

To examine atmospheric conditions in the study regions, pressure vertical coordinate profiles from ERA-Interim (Dee et al. 2011) were extracted over the study regions every 6 h over the period 1998–2013 (Table 1). Profiles of specific humidity and wind were used to calculate cross-barrier moisture flux according to a barrier rotation angle (Table 1). To gain insight into conditions relevant to precipitation processes in these regions, ERA-Interim profiles were considered over 6-h periods when the TRMM Multisatellite Precipitation Analysis 3B42, version 7 (Huffman et al. 2007), domain-averaged 6-h precipitation rate was >0.5 mm h^{-1} (which is 8.8% of the total 6-h periods and 61.8% of the total rainfall

accumulation in all boxes). ERA-Interim profiles were only considered at model pressure levels less than surface pressure and were only composited if >40% of the observations at that level were valid observations.

4. Results

Precipitation–elevation relationships from the TRMM PR climatology differ among precipitation regimes (Fig. 2). The tropical regime (NAN, HIM, and NGA) is characterized by a broad moderate-elevation precipitation maxima beginning at ~200-m elevation and reaching a peak value at ~1000 m (closer to 2000 m for HIM). The trade wind regime (EAU and NEB) has a near–sea level precipitation maximum, with precipitation rates decreasing with elevation to about 200-m elevation and fairly constant above. Regions experiencing monsoon-dominated precipitation yield two distinct patterns. WGA and MYA have substantial sea level precipitation rates and relatively constant precipitation rates above ~400-m elevation on the windward side. These relationships are observed on the windward side of the topography: the lee side is drier and precipitation rates do not strongly vary with elevation. In MEX and AFR, precipitation rates at sea level are low and generally increase with elevation at least to ~1500–2000 m, consistent with findings of Nesbitt et al. (2008) and Hirpa et al. (2010). We separate our study regions into wet monsoon regimes (WGA and MYA) with low-elevation precipitation maxima and dry monsoon regimes (MEX and AFR) where increasing precipitation increases with elevation.

In Fig. 3, CFADs of TRMM reflectivity profiles are shown for convective and stratiform PR rain classifications. Convective profiles are similar within regimes, with the largest variability among regions in the tropical regime, which is perhaps not surprising given the widely varying topography, land cover, and meteorological conditions (including aerosol environments) within this regime. Both
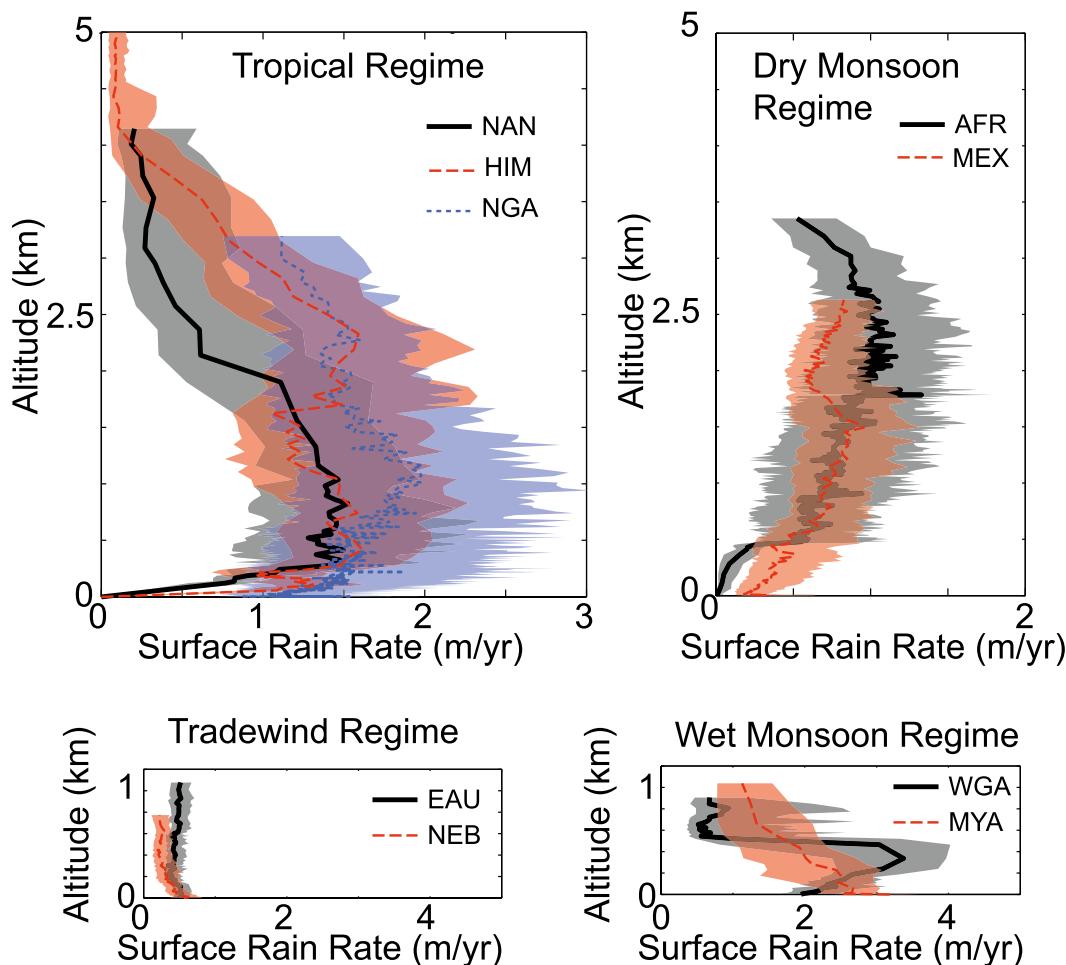
FIG. 2. TRMM PR average annual precipitation plotted as a function of elevation for the study areas. Lines indicate mean values, and shaded regions show one std dev above and below the mean.

the tropical and dry monsoon regions have a deep convective mode, with the deepest convection marked by high probabilities of elevated reflectivity in MEX, AFR, and HIM (e.g., the 0.1 frequency contour crosses near 40 dBZ at 10 km). Outside of these areas, reflectivity probabilities are significantly lower above 8 km. In the trade wind and wet monsoon regions, convective profiles are dominated by high convective reflectivity value probability below the melting level (~4.5–5 km), indicating a low frequency of intense convection in these regions. The presence of shallow convection in all regimes except the dry monsoon (MEX and AFR) regime is suggested by the presence of a low reflectivity peak that maximizes near 20 dBZ at 2-km height. This peak contains the clear majority of reflectivity profiles for the trade wind (EAU and NEB) and wet monsoon (WGA and MYA) regimes and a near plurality of low-level reflectivity frequency in the NAN and NGA, with a somewhat lower frequency in HIM. This second peak

is not present in the dry monsoon (MEX and AFR) regime, indicating the dominance of deep convection as a convective mode in these regions. Note that in both MEX and AFR, the relative frequency of low-level reflectivities in excess of 40 and 50 dBZ near 3 km is higher than any other region (connected with a deep convective signature aloft), while the trade wind and wet monsoon regimes are characterized by high reflectivities at low levels near 2 km, with reflectivities decreasing rapidly with height, indicating a prevalence of low-level, warm rain–dominated precipitation processes. The tropical regime appears to be a blend of these two processes.

The stratiform CFADs are much less variable between regions, likely relating the commonality of the precipitation process of ice crystal growth and aggregation aloft and particle melting (with the associated radar bright band). The structure above the melting level is remarkably similar across all regimes, despite differences in the convective structures. Below the melting
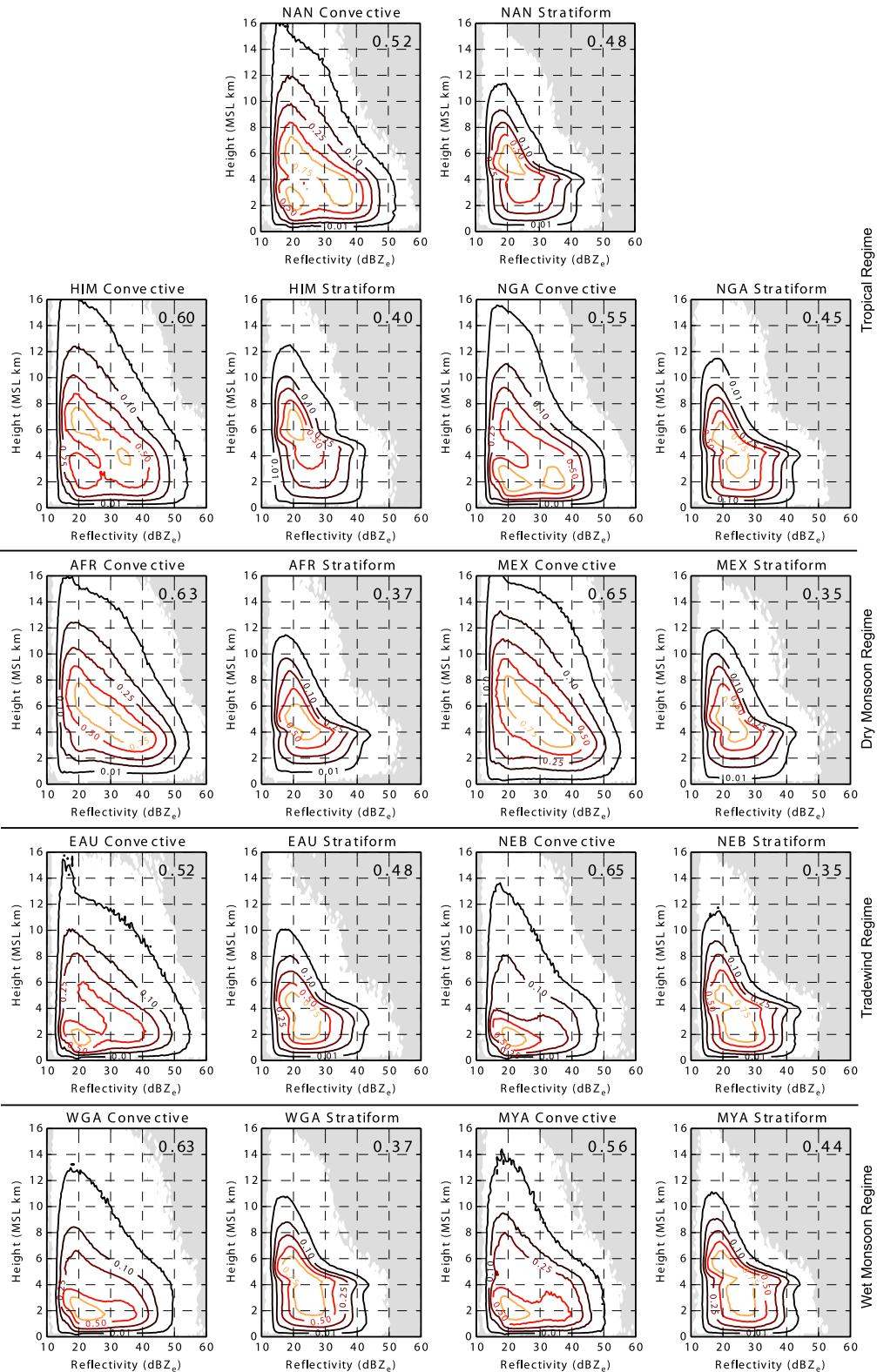
FIG. 3. CFADs of convective and stratiform TRMM radar reflectivity (dBZ_e) within the study regions. The bin size in height is 0.25 km, and in reflectivity is 0.5 dBZ_e. The boldface values in the upper right are the fractions of near-surface rain volume from each category.
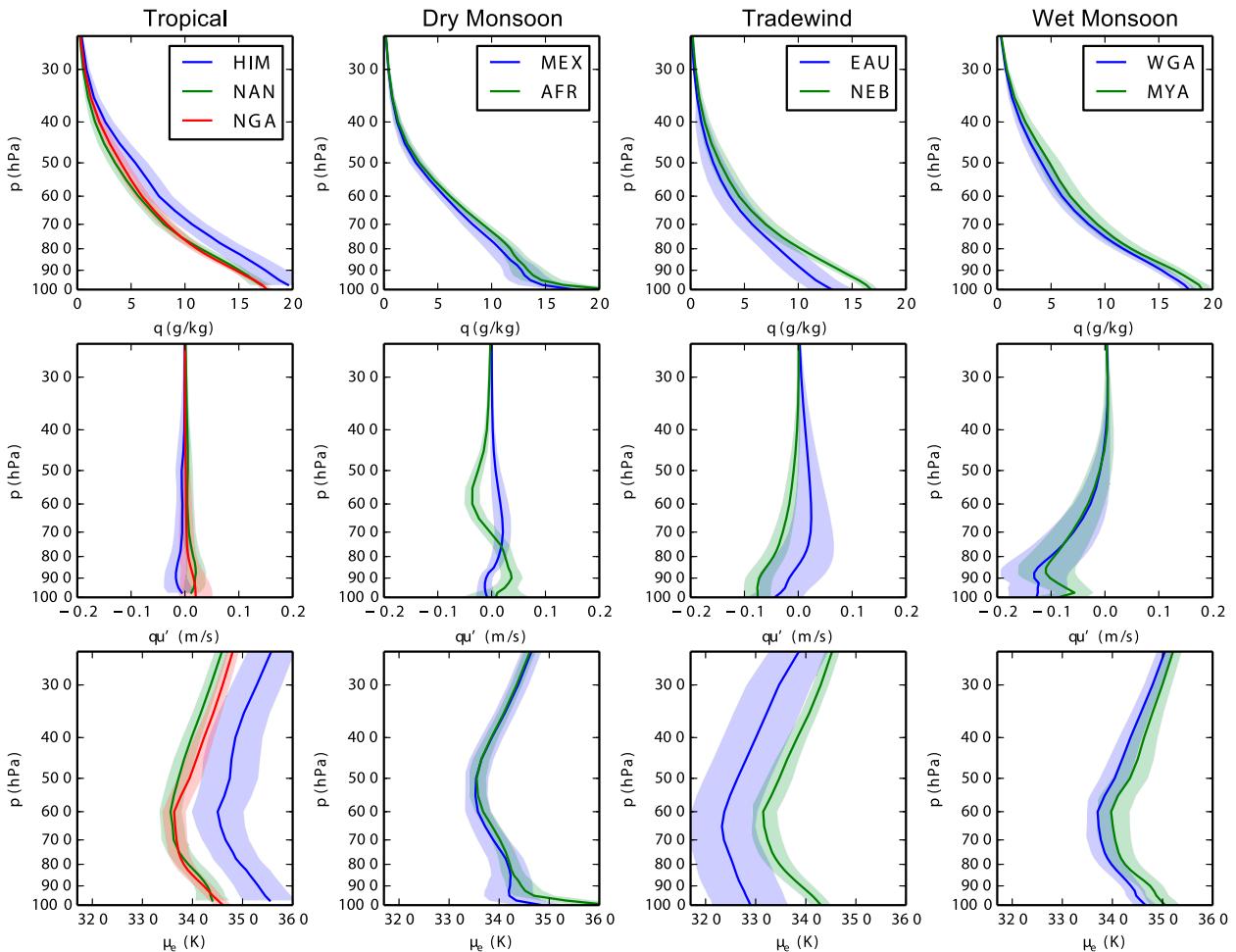
FIG. 4. (top) Vertical profiles of specific humidity, (middle) cross-barrier moisture fluxes, and (bottom) equivalent potential temperature during precipitation events from ERA-Interim. Lines show the mean value, and shaded regions show one std dev above and below the mean.

level, there are more pronounced differences between regimes: reflectivity decreases most strongly in the dry monsoon (MEX and AFR) regime, while in the wet monsoon (WGA and NGA) regime, reflectivity is more likely to extend toward the surface. These differences likely indicate that raindrop evaporation is more significant in the dry monsoon regime than in the wet monsoon regime, which is consistent with differences in near-surface humidity described below.

The four precipitation regimes identified correspond with differences in the mean vertical profiles of specific humidity q, cross-barrier moisture fluxes qu', and profiles of equivalent potential temperature θ_e during precipitation events represented by ERA-Interim (Fig. 4). Profiles in the tropical (HIM, NAN, and NGA) regime are characterized by deep moisture, little cross-barrier moisture flux, and similar stability profiles as indicated with θ_e. The HIM region has the highest θ_e values of any

region examined, consistent with the strong moisture fluxes in the Indian summer monsoon (e.g., Fasullo and Webster 2003). The dry monsoon (MEX and AFR) regime has lower specific humidity than the tropical regime, particularly above the lowest levels. In both AFR and MEX, cross-barrier moisture flux is larger on average than any of the tropical regions, indicating the presence of vertical shear; θ_e profiles are similar to the tropical regime, with very high values in the lowest levels (indicating low-elevation regions have high moisture). In the trade wind (EAU and NEB) regime, drier midlevels are present and seen in low θ_e values near 600 hPa. Low-level, cross-barrier moisture transport is evident, especially in NEB. In the wet monsoon (WGA and MYA) regime, deep moisture is present, along with strong cross-barrier moisture fluxes; however, relatively high midlevel stability likely limits convection to shallow heights.

5. Discussion and conclusions

Analysis of TRMM PR data and ERA-Interim results indicates that, relative to the midlatitudes, precipitation maxima in the tropics tend to occur at lower elevations and precipitation begins to decrease with elevation at moderate elevation. This behavior contrasts with the well-established midlatitude pattern in which climatological precipitation rates increase with elevation (e.g., Smith 1979; Roe 2005; Barry 2008). Evaluation of a larger number of sites using both remote sensing and ground-based gauging is needed to refine understanding of trends in precipitation–elevation relationships across the tropics and to further assess the causes of these patterns.

The variability in precipitation–elevation relationships across the tropics corresponds with distinct precipitation regimes that are influenced by the prevailing flow, vertical distribution of atmospheric moisture, atmospheric conditional instability, and convective mode. The tropical (NAN, HIM, and NGA) regime was identified as the behavior characteristic of high mountains in the tropics in the absence of other strong forcing factors. The precipitation–elevation relationship in these settings includes a broad precipitation maximum between ~1000- and 2000-m elevation (Fig. 2). The lack of appreciable cross-barrier moisture flux suggests that lifting and precipitation are initiated by topographically triggered convection with a deep and a shallow mode, as shown by the reflectivity CFADs (Fig. 3) rather than forced ascent (Fig. 4), and the broad precipitation maximum up to 2000 m is consistent with the presence of both shallow and deep convection (Fig. 2).

The trade wind (NEB and EAU) regime is characterized by a near–sea level precipitation maximum and nearly constant precipitation above ~200 m (Fig. 2). This pattern is hypothesized to result from shallow convection (Fig. 3), capped by dry, low θ_e air aloft. The presence of positive cross-barrier moisture fluxes at low elevations suggests a role for forced ascent in triggering precipitation at low levels (Fig. 4), consistent with results from Dominica reported by Smith et al. (2012).

In areas dominated by monsoons, we identify two distinct regimes, a wet monsoon regime, in which a low-elevation precipitation maximum is observed (MYA and WGA), and a dry monsoon regime, in which precipitation rates increase with elevation to altitudes of 1500–2500 m (AFR and MEX; Fig. 2). Specific humidity profiles from these regions suggest a reason for the contrasting behavior. In the dry monsoon regime, q is high (low) at low (high) altitudes, while in the wet monsoon regime, it is high at midlevels (Fig. 4). In the dry monsoon regime, we suggest that when monsoon and topographic circulations (in relatively low cross-barrier moisture flux) draw air that is moist at low levels yet dry at midlevels, an intense deep convective mode develops, and strong downdrafts develop that organize convection in the presence of vertical shear, in addition to evaporating stratiform rain in dry low- to midtropospheric air (Fig. 4). Indeed AFR and MEX are characterized by high convective rain fractions and intense, organized convective systems (Nesbitt et al. 2006). In this regime, the characteristic life cycle of terrain-triggered convective systems likely plays an important role in determining the elevation of the precipitation maximum. In the wet monsoon regions, cross-barrier moisture fluxes are significant, suggesting that convection and stratiform rain are enhanced over regions of terrain-induced moisture flux convergence (Fig. 4). The shallow nature of the convection is limited by a stable θ_e profile, and the profile suggests tight precipitation–terrain coupling with forced ascent, contributing to a low-elevation precipitation maximum (Nesbitt and Anders 2009).

REFERENCES

Adams, D. K., and A. C. Comrie, 1997: The North American Monsoon. *Bull. Amer. Meteor. Soc.,* **78,** 2197–2213, doi:10.1175/1520-0477(1997)078<2197:TNAM>2.0.CO;2.

Anders, A. M., G. H. Roe, B. Hallet, D. R. Montgomery, N. J. Finnegan, and J. Putkonen, 2006: Spatial patterns of precipitation and topography in the Himalaya. *Spec. Pap. Geol. Soc. Amer.,* **389,** 39–53.

——, ——, D. R. Durran, and J. R. Minder, 2007: Small-scale spatial gradients in climatological precipitation on the Olympic Peninsula. *J. Hydrometeor.,* **8,** 1068–1081, doi:10.1175/JHM610.1.

Barry, R. G., 2008: *Mountain Weather and Climate.* Cambridge University Press, 506 pp.

Colberg, J. S., and A. M. Anders, 2014: Numerical modeling of spatially-variable precipitation and passive margin escarpment evolution. *Geomorphology,* **207,** 203–212, doi:10.1016/j.geomorph.2013.11.006.

Dee, D. P., and Coauthors, 2011: The ERA-Interim reanalysis: Configuration and performance of the data assimilation system. *Quart. J. Roy. Meteor. Soc.,* **137,** 553–597, doi:10.1002/qj.828.

Fasullo, J., and P. J. Webster, 2003: A hydrological definition of Indian monsoon onset and withdrawal. *J. Climate,* **16,** 3200–3211, doi:10.1175/1520-0442(2003)016<3200a:AHDOIM>2.0.CO;2.

Figueroa, S. N., and C. A. Nobre, 1990: Precipitation distribution over central and western tropical South America. *Climanalise,* **5,** 36–45.

Gadgil, S., 2003: The Indian monsoon and its variability. *Annu. Rev. Earth Planet. Sci.,* **31,** 429–467, doi:10.1146/annurev.earth.31.100901.141251.

Giambelluca, T. W., Q. Chen, A. G. Frazier, J. P. Price, Y.-L. Chen, P.-S. Chu, J. K. Eischeid, and D. M. Delparte, 2013: Online rainfall atlas of Hawai'i. *Bull. Amer. Meteor. Soc.,* **94,** 313–316, doi:10.1175/BAMS-D-11-00228.1.

Gochis, D. J., S. W. Nesbitt, W. Yu, and S. Williams, 2009: Comparison of gauge-corrected versus non-gauge corrected satellite-based quantitative precipitation estimates during the 2004 NAME Enhanced Observing period. *Atmósphera,* **22,** 69–98.

Goswami, B. N., V. Krishnamurthy, and H. Annamalai, 1999: A broad-scale circulation index for the interannual variability of the Indian summer monsoon. *Quart. J. Roy. Meteor. Soc.,* **125,** 611–633, doi:10.1002/qj.49712555412.

Hirpa, F. A., M. Gebremichael, and T. Hopson, 2010: Evaluation of high-resolution satellite precipitation products over very complex terrain in Ethiopia. *J. Appl. Meteor. Climatol.,* **49,** 1044–1051, doi:10.1175/2009JAMC2298.1.

Huffman, G. J., D. T. Bolvin, E. J. Nelkin, and D. B. Wolff, 2007: The TRMM multisatellite precipitation analysis (TMPA): Quasi-global, multiyear, combined-sensor precipitation estimates at fine scales. *J. Hydrometeor.,* **8,** 38–55, doi:10.1175/JHM560.1.

Kousky, V. E., 1980: Diurnal rainfall variation in Northeast Brazil. *Mon. Wea. Rev.,* **108,** 488–498, doi:10.1175/1520-0493(1980)108<0488:DRVINB>2.0.CO;2.

Lauer, W., 1975: Klimatische Grundzüge der Höhenstufung tropischer Gebirge. *Tagungsbericht und wissenschaftliche Abhandlungen,* Vol. 40, F. Steiner, 76–90.

Lauscher, F., 1976: Weltweite Typen der Höhenabhängigkeit des Niederschlags. *Wetter Leben,* **28,** 80–90.

Nesbitt, S. W., and A. M. Anders, 2009: Very high resolution precipitation climatologies from the Tropical Rainfall Measuring Mission Precipitation Radar. *Geophys. Res. Lett.,* **36,** L15815, doi:10.1029/2009GL038026.

——, R. Cifelli, and S. A. Rutledge, 2006: Storm morphology and rainfall characteristics of TRMM precipitation features. *Mon. Wea. Rev.,* **134,** 2702–2721, doi:10.1175/MWR3200.1.

——, D. J. Gochis, and T. J. Lang, 2008: The diurnal cycle of clouds and precipitation along the Sierra Madre Occidental during the North American Monsoon Experiment: Implications for precipitation estimation in complex terrain. *J. Hydrometeor.,* **9,** 728–743, doi:10.1175/2008JHM939.1.

Nicholson, S. E., 2000: The nature of rainfall variability over Africa on time scales of decades to millennia. *Global Planet. Change,* **26,** 137–158, doi:10.1016/S0921-8181(00)00040-0.

Prat, O. P., and A. P. Barros, 2010: Ground observations to characterize the spatial gradients and vertical structure of orographic precipitation—Experiments in the inner region of the Great Smoky Mountains. *J. Hydrol.,* **391,** 141–156, doi:10.1016/j.jhydrol.2010.07.013.

Rao, V. B., M. C. De Lima, and S. H. Franchito, 1993: Seasonal and interannual variations of rainfall over eastern northeast Brazil. *J. Climate,* **6,** 1754–1763, doi:10.1175/1520-0442(1993)006<1754:SAIVOR>2.0.CO;2.

Roe, G. H., 2005: Orographic Precipitation. *Annu. Rev. Earth Planet. Sci.,* **33,** 645–671, doi:10.1146/annurev.earth.33.092203.122541.

Sawyer, J. S., 1956: The physical and dynamical problems of orographic rain. *Weather,* **11,** 375–381, doi:10.1002/j.1477-8696.1956.tb00264.x.

Smith, R. B., 1979: The influence of mountains on the atmosphere. *Advances in Geophysics,* Vol. 21, 87–230, doi:10.1016/S0065-2687(08)60262-9.

——, and Coauthors, 2012: Orographic precipitation in the tropics: The Dominica Experiment. *Bull. Amer. Meteor. Soc.,* **93,** 1567–1579, doi:10.1175/BAMS-D-11-00194.1.

Sumner, G., and M. Bonell, 1986: Circulation and daily rainfall in the North Queensland wet seasons 1979–1982. *J. Climatol.,* **6,** 531–549, doi:10.1002/joc.3370060507.

Zhou, J., and K.-M. Lau, 1998: Does a monsoon climate exist over South America? *J. Climate,* **11,** 1020–1040, doi:10.1175/1520-0442(1998)011<1020:DAMCEO>2.0.CO;2.